Condition Assessment of Concrete Nuclear Structures Considered for Entombment

Kenneth A. Snyder

NISTIR 7026

Condition Assessment of Concrete Nuclear Structures Considered for Entombment

Kenneth A. Snyder

Materials and Construction Research Division
Building and Fire Research Laboratory

U.S. DEPARTMENT OF COMMERCE
Donald L. Evans, *S*ecretary

TECHNOLOGY ADMINISTRATION
Phillip J. Bond, *U*ndersecretary of Commerce for Technology

NATIONAL INSTITUTE OF STANDARDS AND TECHNOLOGY
Arden L. Bement, Jr., *D*irector

Condition Assessment of Concrete Nuclear Structures Considered for Entombment

K.A. Snyder

July 14, 2003

VERSION: 20030108:1545

Abstract

This Report summarizes work to date on a project for the U.S. Nuclear Regulatory Commission to develop guidelines for the chemical and material assessment of an existing structure considered for entombment. In addition, a rational means for performing a probabilistic calculation are addressed. This report is limited to materials issues as they relate to the overall performance of the structure. Structural issues such as the presence of cracks and the location of rebars are discussed only in the context of their effect on transport.

The assessment is composed of a preliminary material assessment, followed by a probabilistic calculation of the service life. The material assessment will rely heavily on both the permeability of the intact concrete and the characterization of any existing cracks. The contribution of cracks to transport is considered independently from the intact concrete, and the bulk properties (intact concrete plus cracks) are estimated by combining the two effects using a composite model. Another aspect of the condition assessment of the concrete barrier is the evaluation of nondestructive techniques (NDT) as candidates for characterizing existing cracks, and other transport pathways, in the entombment structure. This aspect will be addressed in a companion report.

An important component of the effort to estimate the concrete material properties is the probability density function used to characterize the distribution in their expected values. The "tail" of the distribution has the greatest influence on the overall performance, and, therefore, it should receive attention in the analysis. A number of suitable distributions are considered for their use in characterizing various concrete material properties.

Contents

List of Figures

List of Tables

1 Overview

Entombment may be considered as a decommissioning option for reactor components and other nuclear structures so that the licenses for facilities on which these structures reside may be terminated. Prior to the entombment process, the nuclear facility permanently ceases operations and spent fuel is removed. After preliminary decommissioning activities are completed, activities that may include the removal of a small volume of highly radioactive material, remaining radioactively contaminated components may be entombed within the structure using an engineered barrier system that could include filling the structure with cement, absorbant grouts, or infills. Entombment may reduce exposure to the workers and to the public during decommissioning because only a small volume fraction of the structure has to be transported to a waste isolation facility. An important consideration for decommissioning is that the existing concrete nuclear structure is a primary barrier between its remaining contents and the environment.

As a consequence, however, the entombed nuclear concrete structure may be the final barrier between the contaminated material and the environment. Therefore, a careful assessment of the future performance of the entombed concrete structure is vital to assured isolation. The assessment involves characterizing the existing condition of the concrete structure and the chemistry of the ground water within the surrounding soil. The condition of the existing structure will be characterized primarily by the relevant transport coefficients, and the geometry of the critical concrete elements. The surrounding ground water will have to be tested to determine the concentration of each dissolved ionic species.

The final service life estimate will be probabilistic, based on parameter uncertainty. Therefore, it will be important to fully characterize the uncertainty distribution of the relevant transport coefficients. This will require sufficient sampling to assure that the "tails" of the distribution are known to a satisfactory level, for the "tail" of the probable outcomes will depend directly on them.

As will be shown, it will be vital to carefully examine the structure for the existence of cracks. When advective (Darcy) flow needs to be considered, cracks are an important factor in estimating the total transport through the concrete. Three crack parameters are significant: crack width at the surface, the number of cracks per unit length, and the depth of crack penetration. Although the permeability of a crack is a quadratic function of the crack width, the depth of crack penetration is, by far, the most important crack parameter determining the overall permeability of the structure.

In addition to the existing condition, one should also consider the possible changes in the structure and its environment. Changes in the loading within the structure may propagate existing cracks, or induce the formation of new cracks. Changes in the environment may induce degradation mechanisms that can create internal stresses. These possibilities, and their effect on transport through the structure, must be considered.

Subsequent to the assessment of the concrete and the characterization of existing cracks, one can make an estimate of the service life based on the 4SIGHT computer program [1, 2]. The program attempts to consider as many material and environmental properties as possible to estimate the time until the onset of a degration mechanism.

The service lifetime estimation is based on a reactive transport algorithm that correctly models the interaction of ions within the pore solution [2,3]. Because the expected service lifetime of massive structures is expected to be measured in decades or centuries, the time between the onset of degration and the development of sufficient stress to produce failure is assumed to be an insignificant proportion of the overall service lifetime.

2 Condition Assessment

The objective of the concrete structure condition assessment is to quantify the relevant material properties required to estimate the remaining service life. The primary cause of premature failure of a concrete structure is chemically induced mechanical degradation. Generally, the deleterious chemical reactions are due to diffusion of ionic species. Therefore, assessment of the concrete depends on its present condition and the spatial distribution of diffusing ionic species.

In addition to characterizing the present condition of the structure, the assessment must also estimate the uncertainty in the relevant material parameters. This involves choosing a probability distribution that accurately characterizes the dispersion in values of the parameter in question. Given that the chosen underlying probability distribution is suitable for the particular property, the parametric approach has the advantage of reducing the number of samples required for characterizing the range of possible values expected; in effect, it becomes easier to characterize the "tails" of the distribution.

In the following, each of the relevant material parameters is described and methods are reviewed for measuring or estimating the values and uncertainties, and for characterizing the underlying distribution. Arguments are given for choosing particular distributions to characterize a parameter.

2.1 Probability Distribution

Probabilistic calculations require random values for the material parameters. The user must choose a probability density function (PDF) for characterizing the dispersion of expected values. Some distributions have longer "tails" than others, so the choice of the PDF is important because the failure scenarios likely depend upon the extremes in the values of one or more of these parameters.

Currently, there are four PDFs to choose from: Dirac delta function, uniform (top hat) distribution, normal (Gaussian) distribution, and lognormal. The Dirac delta function allows the user to specify a fixed value for a parameter [4]. The uniform distribution is for properties that can be bounded. The normal distribution is for properties that vary over a factor of two or less. The lognormal distribution is for properties that vary over orders of magnitude [5].

2.2 Geometry

Although material parameters are critical to the assessment, there are two structural geometrical parameters of interest: concrete element thickness and the location of steel components such as reinforcement. The concrete element thickness determines the spatial boundary conditions. There are methods for determining this dimension: direct observation, nondestructive techniques (e.g., sound wave propagation), and construction schematics. The location of steel reinforcement, if present, effects the time until the possibility of corrosion initiation. In the presence of chloride ions, steel corrosion is likely when the chloride concentration in the pore solution exceeds a critical concentration.

2.2.1 Expected distribution

The geometrical quantities of interest are the concrete element dimensions and the location of steel elements that, with sufficient corrosion, could lead to mechanical failure of the structure. Because concrete elements and the location of steel components were established from technical construction plans, the actual dimensions should be relatively close to the designed values. Therefore, one would expect that the underlying distribution should be normal, with relatively little variance.

2.2.2 Direct measurement

The most reliable determination of concrete element dimension is direct physical observation. These observations can be compared to the original plans for compliance determination.

2.2.3 Indirect measurement

For cases involving inaccessible concrete elements, nondestructive techniques may be suitable alternatives [6]. As for direct measurement, the nondestructive testing results can be compared to the original construction plans for independent verification. Alternatively, the construction plans, in the absence of any measurements from the structure, could be used to establish dimensions. This approach, however, gives no assurances that the dimensional requirements have been met.

2.3 Water:Cement Ratio

At the time the concrete mixture is formulated, the most important parameter controlling the overall properties of the concrete is the water:cement (or water:cementitious for the case of concretes using supplemental pozzolanic materials) ratio. As such, knowledge of this ratio can be very helpful for inferring material properties that might not otherwise be obtainable. Water:cement ratio controls the concrete compressive strength, permeability, and diffusivity.

Concrete for large projects such as a nuclear facility typically is batched at a plant using computer controlled delivery systems. Although attempts are made to produce a consistent product, variations in the water:cement ratio are to be expected. One could expect that a concrete producer with stringent quality controls should be able to produce a concrete with minimal variation in the water:cement ratio.

Variations in the water:cement ratio can arise during both the batching and the construction. There naturally will be small variations in the batching volumes, resulting in variations in both the aggregate volume and water:cement ratio. During normal concrete production, however, the concrete trucks are rinsed clean with water before the next load. While on transit to the construction site, and while waiting at the construction site, the mixture may lose water due to evaporation. Further, if the workability of the concrete has decreased, the truck driver may feel compelled to add water to the mixture to regain the lost workability.

2.3.1 Expected distribution

A number of possible scenarios exist that may lead to variations in water:cement ratio. According to the American Concrete Institute (ACI), the tolerance for total water content is 3 % and the tolerance for cementitious materials ranges from 1 % to 4 % depending on the scale limits [*"Standard Specifications for Tolerances (ACI 117-90),"* in Part 2 of Ref. [7]]. Therefore, the water:cement ratio variability should be in the range 3 % to 5 %. At these percentages, it would seem plausible to characterize the water:cement ratio by a normal distribution.

The shortest service lifetimes will likely coincide with the largest possible values for water:cement ratio. These larger values lead to greater porosities, larger permeabilities and lower compressive strengths, and more rapid transport of aggressive ionic species.

2.3.2 Direct measurement

Direct measurement of water:cement ratio of a fully hydrated concrete specimen is a difficult process. It typically requires a scanning electron microscope (SEM) analysis of the hydrated paste within the concrete. In addition, certain assumptions must be made. Fortunately, an easier way to characterize the variability in the water:cement ratio, and also the overall quality, is to make compressive strength measurements. Compressive strength measurements can be obtained from a straightforward test procedure and are the default means of quality control at the time of construction. Moreover, for a nuclear structure, the compressive strength measurements at the time of construction should have been recorded, and can serve as an indirect measurement to complement compressive strength testing at the time of entombment.

2.3.3 Indirect estimation

It is difficult to estimate the water:cement ratio without either the original specified mixture design or strength tests. The water:cement ratio could be inferred from permeability measurements, but the relationship is not as reliable as for compressive strength.

2.4 Permeability

The permeability of the intact portion of the concrete is probably the single most important parameter for assessing the future performance of an engineered barrier system. Typically, the permeability of concrete is on the order of 10^{-17} m^2 to 10^{-18} m^2. Although the measurement of concrete permeability has been reported in the concrete materials literature, measurements on specimens with low water:cement ratios having exceedingly low permeabilities might have to rely on novel dynamic techniques developed for geological research [8, 9].

The permeability of concrete is a strong function of the water:cement ratio (w/c). Unfortunately, even at a fixed value of w/c, the measured permeability of various concretes can still vary over orders of magnitude [10]. Therefore, although knowing the w/c

of the concrete used in the structure is helpful, predictions based on published data still contain uncertainty that spans orders of magnitude.

The sample-to-sample variation within a given structure is still unpredictable and must be measured directly. Here, the analyst must be careful when choosing the proper PDF. A small number of measurements may not exhibit sufficient skewness that would help to distinguish between a normal and lognormal distribution.

2.4.1 Expected distribution

Permeabilities can span orders of magnitude, even for repeated measurements on samples with nominally the same water:cement ratio. Therefore, the lognormal distribution is the preferred candidate for characterizing the expected range of values used in a probabilistic calculation. The parameters of the distribution can be determined by taking the (base-10) logarithm of the measured permeabilities and then calculating the mean and standard deviation of the logarithms.

2.4.2 Direct measurement

Direct measurements of permeability are divided between equilibrium and dynamic measurements. Equilibrium measurements typically consist of applying a hydrostatic pressure difference across a specimen and measuring the flow rate through the sample. The analysis and estimate of the permeability is very straightforward from the experimental values. Unfortunately, for very low permeabilities ($< 10^{-18}$ m^2), this approach has practical limitations.

The dynamic approach uses a slightly different experimental setup [9], and requires more sophisticated analysis [8]. Reservoirs are located at both ends of the sample and the pressure in one reservoir is increased by a step function. As the liquid flows through the specimen, the pressure in both reservoirs approaches an equilibrium value. The permeability of the sample is estimated from the rate of pressure change in both reservoirs. This method has been used on geological samples with permeabilities below 10^{-20} m^2.

2.4.3 Indirect estimation

Indirect estimates of the permeability are not recommended. There is no single independent material parameter from which one can make a reliable estimate of the permeability. Only by direct observation can one make assurances that the distribution of possible permeabilities is characterized sufficiently well.

2.5 Formation Factor

The formation factor is a useful material property for characterizing both diffusive and advective transport in cementitious systems. The formation factor F is the ratio of the pore solution conductivity σ_p to the concrete conductivity σ_c:

$$F = \frac{\sigma_p}{\sigma_c} \tag{1}$$

This approach has the advantage that conductivity is a relatively easy and accurate experimental measurement.

2.5.1   Expected distribution

Even though typical values for the formation factor of concretes range from 100 to 1000, the values measured from a single structure may vary over a relatively small range. Only a careful analysis of the data will reveal whether the appropriate distribution should be the normal or lognormal distribution.

2.5.2   Direct measurement

Direct determinations of the formation factor consist of separate tests for the pore solution and the concrete conductivities. The pore solution conductivity can be determined from samples obtained from pore fluid expression [11]. The pore solution conductivity can then be measured directly using a solution conductivity meter. Otherwise, elemental techniques such as ion chromatography can be used to determine the concentration of majority ionic species such as OH^-, K^+, and Na^+, and the conductivity estimated from these concentrations.

The concrete conductivity can be most easily measured using the apparatus for the ASTM C 1202 Rapid Chloride Test. It has been shown that the instantaneous current is proportional to the sample conductivity, to within an acceptable uncertainty [12]. After the concrete conductivity measurement, pore expression can be used to extract a sample of the pore solution, and the pore solution conductivity can be determined as described above.

2.5.3   Indirect estimation

There are two indirect methods for estimating the formation factor. The first uses a model such as the NIST microstructural model [13] to estimate the formation factor from the water:cement ratio and degree of hydration. The other makes a direct measurement of the bulk conductivity (because it is a simple test) and estimates the pore solution composition. The indirect method that relies on a model for the formation factor is less reliable because the results can be a function of the types of supplementary cementitious materials (fly ash, silica fume, etc.) present.

The second indirect method contains less uncertainty because the variability in the pore solution conductivity is fairly small. For ordinary portland cement pastes, the pore solution conductivity typically varies between 10 S/m and 20 S/m. The addition of supplemental cementitious materials can have an effect, but the conductivity will still typically be above 5 S/m.

2.6   Pore Solution Composition

The rate of ionic transport in porous media can depend upon the chemical composition of the pore solution. Therefore, a meaningful assessment requires characterizing the pore

solution composition. Fortunately, the pore solution is typically composed of only a few inorganic ionic species: OH^-, K^+, Na^+, Cl^-, SO_4^{2-}, Mg^{2+}, etc. These species can be detected using a number of established analytical techniques such as atomic absorption and ion chromatography.

2.6.1 Direct measurement

The direct assessment of the pore solution composition is a simple analytical chemistry problem, but a more difficult physical testing problem. The most direct means of extracting a sample of the pore solution is by pore expression. Unfortunately, an aged specimen exposed to atmospheric conditions presents experimental difficulties: it has relatively little pore solution remaining, and atmospheric exposure can evaporate a portion of any remaining pore solution. If, however, a sample can be obtained from within the concrete element, the sample will probably be saturated to its maximum extent.

2.6.2 Indirect estimation

The best means of estimating the pore solution is to use a model such as that by Taylor [14]. The estimate based on the Taylor model can be simplified by assuming that at 30 years the individual phases have completely hydrated, as is allowed by the initial water:cement ratio.

The estimate largely depends on the oxide content of the cement and the initial water:cement ratio. From the oxide content, one can estimate the total number of moles μ_T of a particular element per 100 g cement. From this estimate, Taylor assumes that the number of immediately soluble moles μ_{sol} is 35 % of the total sodium content and is 70 % of the total potassium content.

For water:cement ratios greater than approximately 0.40, the cement paste can completely hydrate because there is sufficient water available initially and there is sufficient initial capillary pore volume to accommodate the net increase in volume of solids produced during hydration. For a 30 year-old structure with a water:cement ratio greater than 0.40, the Taylor model assumes that all of the available sodium and potassium will have been released. The maximum degree of hydration α_{max} for an ordinary portland cement (OPC) paste is a function of water:cement ratio ϵ:

$$\alpha_{max} = \mathrm{MIN}(2.5\epsilon, 1)$$

The number of moles released μ_r for an element is then a function of the total number of moles μ_T and the immediately soluble moles μ_{sol}:

$$\mu_r = \mu_{sol} + \alpha_{max}\left(\mu_T - \mu_{sol}\right)$$

This relationship does not account for the different rates of hydration for the cement phases.

The mass of water (kg) per 100 g cement is the water:cement ratio divided by 10. The molality m_i of the i-th ionic species is the ratio of moles of element released μ_r to

the mass of water, per 100 g cement:

$$m_i = \frac{\mu_r}{\epsilon/10}$$

The sulfate content is approximated from the molalities m_{Na} and m_K of sodium and potassium, respectively, using an empirical relationship [14]:

$$m_{SO_4} \approx (0.06 \text{ kg/mol}) (m_{Na} + m_K)^2 \tag{2}$$

These three species, along with a sufficient hydroxide content to ensure electroneutrality, account for the great majority of the ionic species in cement paste pore solution.
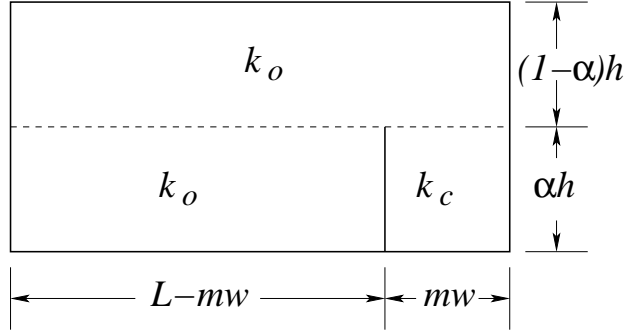
Figure 1: Crack model schematic for a concrete slab with span L, depth h, and containing m cracks, each having width w and penetrating a fraction α into the element. k_o is the permeability of the uncracked concrete, and k_c is the permeability of each crack.

3 Crack Characterization

The properties of intact, uncracked concrete are typically sufficient to ensure isolation of radionuclides for hundreds of years. The presence of cracks, however, can dramatically increase the rate of radionuclide transport. The permeability of uncracked concrete is typically 10^{-18} m^2. A crack composed of plane, parallel walls separated by 10 μm (a very small crack) has a permeability of approximately 10^{-11} m^2, a factor of 10^7 larger than the value for the uncracked concrete. Even after considering the area fraction of the concrete occupied by the crack, the total advective transport can still be greater by a factor of 10. Therefore, it is imperative to carefully characterize the geometry of any cracks present in the structure.

An investigation of the effect cracks have on the total transport was undertaken to evaluate which, if any, of the crack parameters has the greatest influence. Three crack parameters were considered: crack width, number of cracks per unit length of span, and the depth of penetration into the element. First, a composite model of cracks was developed to establish how the cracks participate in the total transport through the element. From that model, the total permeability was calculated as a function of the intact concrete properties and the crack parameters. A simple parallel and series composite model was used, yielding an analytical expression for the total permeability. From this expression, the influence each crack parameter has on the overall permeability was investigated and are discussed in the following sections.

3.1 Composite Model

The influence of cracks on the transport properties of a slab with span L and depth h can be characterized analytically using the schematic shown in Fig. 1. Let there be m cracks, each with width w, perpendicular to the entire the span, and each crack penetrating into the slab a proportion α of the total depth. The permeability of the uncracked concrete is k_o. The permeability of each crack k_c is based on the assumption that the crack walls

are parallel and planar [15]:

$$k_c = \frac{w^2}{12} \tag{3}$$

It is assumed that this equation will be applied to the cracks sufficiently large that a continuum description of the fluid applies and that molecular effects may be neglected.

The total flow through the slab can be estimated by assuming a parallel and series model for the materials. First, the permeability of the cracked and uncracked portion up to the depth αh is calculated. Second, this composite value is put in series with the final $(1 - \alpha)h$ depth of uncracked concrete to determine the overall composite permeability. The composite permeability k_p of the slab to the depth αh is a weighted sum of the two permeabilities (two conductors in parallel):

$$k_p = \left(1 - \frac{mw}{L}\right) k_o + \frac{mw}{L} k_c \tag{4}$$

The bulk permeability k_b of the entire slab is estimated by analogy to electrical conductors in series:

$$k_b = \frac{1 - \alpha}{k_o} + \frac{\alpha}{k_p} \tag{5}$$

This relationship may be simplified, expressing the total bulk permeability k_b as a function of only k_p and α:

$$k_b = \frac{k_o}{1 - (1 - k_o/k_p)\,\alpha} \tag{6}$$

To demonstrate the behavior of Eqn. 6, consider a slab containing 100 μm wide cracks spaced 1 m apart. Each crack penetrates to a fraction α of the total depth h. The permeability of the uncracked concrete is 10^{-18} m^2. The ratio k_b/k_p is plotted in Fig. 2 as a function of the fractional depth α. For this general case of moderate crack width, the ratio of k_b/k_o increases as $(1 - \alpha)^{-1}$.

3.2   Sensitivity Analysis

The objective of the sensitivity analysis is to express the bulk permeability k_b as a function of the crack parameters: crack width w, number of cracks m over span L, and crack penetration fraction α. From this expression, one can make a Taylor expansion for a change Δk_b in the bulk permeability, expressed as a function of changes in the crack parameters: Δw, Δm, and $\Delta \alpha$.

The expression for the bulk permeability k_b is expressed as a function of the crack parameters:

$$k_b = k_o \left[\frac{1 + \beta}{1 + (1 - \alpha)\beta} \right] \tag{7}$$

The intermediate quantity β is a function of the crack width w, the span L, and the number of cracks m:

$$\beta(w, m) = \frac{mw}{L} \left(\frac{k_c}{k_o} - 1 \right) \tag{8}$$

11
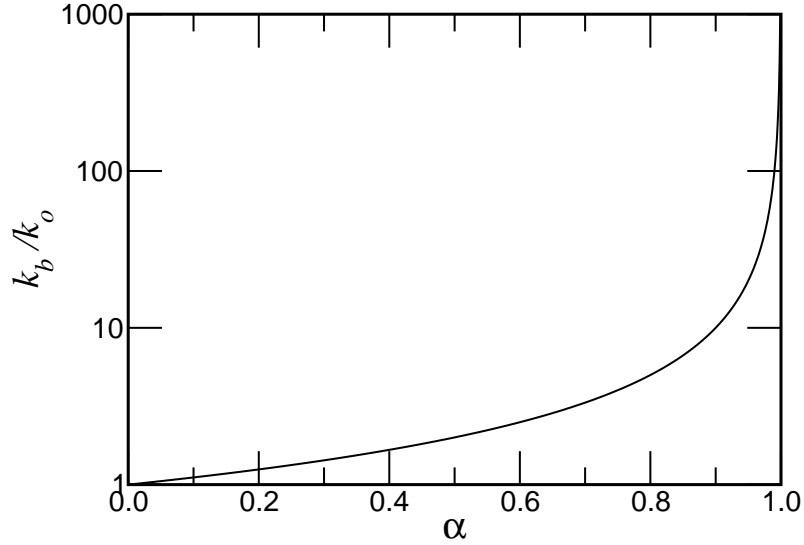
Figure 2: The ratio of the bulk permeability k_b to the intact concrete permeability k_o plotted as a function of crack penetration ratio α. The crack parameters are found in the text.

Given that the permeability k_o of concrete is in the range 10^{-16} m^2 to 10^{-18} m^2, and that cracks in concrete have widths on the order of 10^{-4} m, the parameter β can be simplified by assuming planar, parallel cracks:

$$\beta = \frac{mw^3}{12k_oL} \tag{9}$$

Using the aforementioned example of 10^{-18} m^2 permeability concrete containing 100 μm cracks spaced 1 m apart, the value of β is approximately 10^5.

Using an expression for the bulk permeability k_b as a function of the crack parameters, changes in the bulk permeability Δk_b can be expressed as a Taylor expansion that depends, up to first order, on changes in the crack parameters:

$$\Delta k_b = \frac{dk_b}{dm}\,\Delta m + \frac{dk_b}{dw}\,\Delta w + \frac{dk_b}{d\alpha}\,\Delta \alpha + \cdots \tag{10}$$

The complete differentials are evaluated using the chain rule:

$$\frac{dk_b}{dm} = \frac{\partial k_b}{\partial \beta}\frac{\partial \beta}{\partial m} = k_o\left(\frac{k_b}{k_o}\right)^2 \frac{\alpha\beta}{(1+\beta)^2}\frac{1}{m}$$

$$\frac{dk_b}{dw} = \frac{\partial k_b}{\partial \beta}\frac{\partial \beta}{\partial w} \approx k_o\left(\frac{k_b}{k_o}\right)^2 \frac{\alpha\beta}{(1+\beta)^2}\frac{3}{w} \tag{11}$$

$$\frac{dk_b}{d\alpha} = \frac{\partial k_b}{\partial \alpha} = k_o\left(\frac{k_b}{k_o}\right)^2 \frac{\alpha\beta}{(1+\beta)^2}\frac{1+\beta}{\alpha}$$

Substitution for the differentials into Eqn. 10 gives the following relationship:

$$\frac{\Delta k_b}{k_b} = \left(\frac{k_b}{k_o}\right)\frac{\alpha\beta}{1+\beta}\left[\frac{1}{1+\beta}\frac{\Delta m}{m} + \frac{3}{1+\beta}\frac{\Delta w}{w} + \frac{\Delta\alpha}{\alpha}\right] \tag{12}$$

The fractional penetration α is equivalent to the ratio of the crack penetration depth δ to the total depth h. Therefore, the relative change $\Delta\alpha/\alpha$ is equivalent to the fraction change in the depth:

$$\frac{\Delta k_b}{k_b} = \left(\frac{k_b}{k_o}\right)\frac{\alpha\beta}{1+\beta}\left[\frac{1}{1+\beta}\frac{\Delta m}{m} + \frac{3}{1+\beta}\frac{\Delta w}{w} + \frac{\Delta\delta}{\delta}\right] \tag{13}$$

The effects of changes in the relative number of cracks m and the crack widths w are reduced by a factor of β ($\beta \gg 1$). The $\Delta\delta$ term, however, lacks β in the denominator. Therefore, relative changes in the crack depth can be dramatic, as compared to relative changes in either the crack width or number of cracks.

During condition assessment, efforts should focus on those aspects that are most influential to the overall performance of the structure. The previous result suggests that efforts to characterize cracks in existing structures should concentrate on estimating the depth of crack penetration.

3.3 Crack Parameter Uncertainty

Characterizing the crack parameters during an assessment requires formulating an estimate for both the value of the parameter and its uncertainty. The uncertainties in crack parameters are important because they can be included in the estimated uncertainty in the bulk permeability. A concise definition of uncertainty can be found in either the ISO technical report [16] or the corresponding NIST technical report [17]. For this discussion, the uncertainty will be characterized by the estimated standard deviation s.

In cases where an analytical expression relates an observable quantity to dependent variables, the estimated standard deviation can be calculated from partial differentials and the corresponding uncertainty in the dependent variable [18]. For the case of the bulk permeability k_b, the estimated variance s^2 will be a function of the intact concrete permeability k_o, the number of cracks m, the width of the cracks w, and the relative crack penetration depth α [18, 19]:

$$s_{k_b}^2 = \left(\frac{dk_b}{dk_o}\right)^2 s_{k_o}^2 + \left(\frac{dk_b}{dm}\right)^2 s_m^2 + \left(\frac{dk_b}{dw}\right)^2 s_w^2 + \left(\frac{dk_b}{d\alpha}\right)^2 s_\alpha^2 + \cdots \tag{14}$$

13

The last three differentials can be taken from Eqn. 11 above. The first term in Eqn. 14 may be evaluated using the chain rule:

$$\begin{aligned}
\frac{dk_b}{dk_o} &= \frac{\partial k_b}{\partial k_o} + \frac{\partial k_b}{\partial \beta}\frac{\partial \beta}{\partial k_o} \\
&= k_o\left(\frac{k_b}{k_o}\right)^2\left(\frac{k_o}{k_b} - \frac{\alpha\beta}{(1+\beta)^2}\right)\frac{1}{k_o}
\end{aligned} \tag{15}$$

With all the differential quantities calculated, Eqn. 14 may be rewritten succinctly as a function of the various coefficients of variation (standard deviation divided by value):

$$\begin{aligned}
\left(\frac{s_{k_b}}{k_b}\right)^2 &= \left(\frac{k_b}{k_o}\right)^2\left(\frac{\alpha\beta}{(1+\beta)^2}\right)^2 \\
&\times \left[\left(\frac{k_o}{k_b}\frac{(1+\beta)^2}{\alpha\beta} - 1\right)^2\left(\frac{s_{k_o}}{k_o}\right)^2 + \left(\frac{s_m}{m}\right)^2 + 9\left(\frac{s_w}{w}\right)^2 + (1+\beta)^2\left(\frac{s_\alpha}{\alpha}\right)^2\right]
\end{aligned} \tag{16}$$

As for the sensitivity analysis, the coefficient of variation for α is equivalent to the coefficient of variation in the measured crack penetration depth δ.

The result in Eqn. 16 again demonstrates the need for careful characterization of the crack penetration depth. As in the sensitivity analysis, the contribution of the relative uncertainty in the penetration fraction α is a factor of $(1+\beta)$ greater than the contribution from the relative uncertainty in the other crack parameters. Therefore, to achieve similar magnitudes in the relative contribution from each crack parameter, the relative uncertainty in the crack penetration ratio α would have to be a factor of $(1+\beta)$ smaller than the others.

3.4 Extensive Cracking

In some cases, cracking could be sufficiently severe that the performance of the engineering system cannot be ensured in the existing condition. Fortunately, sealants can be used to penetrate and fill cracks within the concrete. Eliminating the paths of rapid transport within the concrete will dramatically reduce the overall permeability of the structure.

A possible deficiency of synthetic sealants is their unknown long term (over centuries) performance. In the absence of demonstrable proof of the long term performance of the sealant, a suitable monitoring and remediation program for the sealant could be used to gain confidence in the estimated long-term performance.

3.5 Subsequent Crack Initiation

While it is important to characterize existing cracks in the performance assessment prior to entombment, it is also important to enumerate possible causes of subsequent cracking. It has been established that cracks are the primary means of advective (Darcy)

transport through concrete. Therefore, subsequent cracking could decrease the expected performance of a concrete structure.

Subsequent cracking within the concrete can arise from two main causes: mechanical loading, and chemical attack. Mechanically induced cracks could arise from the physical process of entombment as the contents of the structure will be moved around and the volume of the structure filled with grout. The presence of chlorides or sulfates in the groundwater could eventually initiate chemical reactions, leading to internal stresses and, ultimately, cracking.

3.5.1 Mechanically induced cracking

During entombment, a number of construction and demolition processes may induce some measure of added cracking within the concrete structure. These processes may occur during the removal of a portion of the contents or during the possible in-filling of the remaining structure. They include both mechanically and thermally induced cracks. After spent fuel has been removed from the site, and the entombed components returned to the structure, the interior may be grouted with a cementitious material. The remaining entombed structures may be a few stories tall, and cementitious grouts are typically two, or more, times as dense as water. If grouted in a single lift, the hydrostatic forces would be substantial, as would the hoop stresses exerted on the structure. In addition, a cementitious grout would likely involve an exothermic reaction that could generate thermal gradients in the existing concrete structure. Therefore, the grout material selection, placement strategies, and construction sequence must be considered simultaneously.

3.5.2 Chemically induced cracking

Even though an assessment at the time of entombment may reveal no evidence of chemical attack, changes in the environment may occur for a number of reasons. One must consider any environmental changes or new construction that can alter the ground water composition in contact with the concrete. Specifically, sulfate (SO_4^{2-}) can react with aluminate phases to form ettringite. In addition, divalent ionic species such as magnesium (Mg^{2+}) can substitute for calcium within the CSH structure, forming a compound with dramatically reduced mechanical properties.

3.6 Other Major Transport Pathways

In addition to the presence of cracks, there are other possible major transport pathways through the structure. These pathways could include construction joints, sealed joints, conduits, etc. The properties of joints could be characterized, to some degree, by suitable NDE techniques. In addition, NDE could be used to search for unknown pathways such as segregation or casting voids.

4 Sampling Plan

An accurate characterization of the required geometrical and material properties can be obtained only with an adequate sampling plan. Although the material properties can be estimated using existing numerical and computer models, only direct observation can guarantee that the values used in the assessment truly reflect the condition of the structure. Moreover, a proper sampling plan is required to reduce the uncertainty in the material parameters to acceptable levels.

While statistics such as the mean can characterize the central portion of the material parameter distribution, a well-defined means of characterizing the "tail" of the distribution is needed. Generally, if material property values near the 50-th percentile result in estimated failure, the design would be summarily rejected. The expected scenario consists of analyzing cases in which material properties above the 90-th percentile lead to failure. Therefore, one must carefully characterize the "tail" of the material property distribution. The estimated shape of the "tail" will depend both on the underlying distribution for the material property and on the number of samples taken to estimate the parameters of the distribution.

Although the true distribution in the population of material property values may not be known, one could assume an analytical distribution and then test whether the distribution can characterize the data. The two most likely candidates for distributions are the normal (Gaussian) and the lognormal distributions. (For a lognormal distribution, the logarithms are normally distributed.) Both distributions lend themselves to established tests of normality for hypothesis testing. If the data can be shown to originate from a particular distribution, the "tails" of the distribution can be estimated with greater confidence.

4.1 Stratified Random Sampling

A stratified random sampling plan is a means of obtaining information about both the uncertainty in a material property and any spatial dependence that might exist. Figure 3 shows a schematic of the sampling plan. In the figure, a structural element is divided into subsections, represented by dashed lines. Samples, represented by filled circles in the figure, are chosen at random locations within each subsection.

Naturally, not every concrete element is orthorhombic. Therefore, in practice one must make engineering judgments regarding the best way to subdivide a particular element. Furthermore, restrictions on the allowable number of samples will further complicate the process of subdividing the structure. Nonetheless, a sampling plan that follows the philosophy of distributing the samples from various parts of the entire structure will have the best chance of accurately characterizing the condition of the concrete.

4.2 Probabilistic Calculation Requirements

To formulate statistical service lifetime estimates, there has been a universal change from deterministic to probabilistic performance assessment calculations. Deterministic
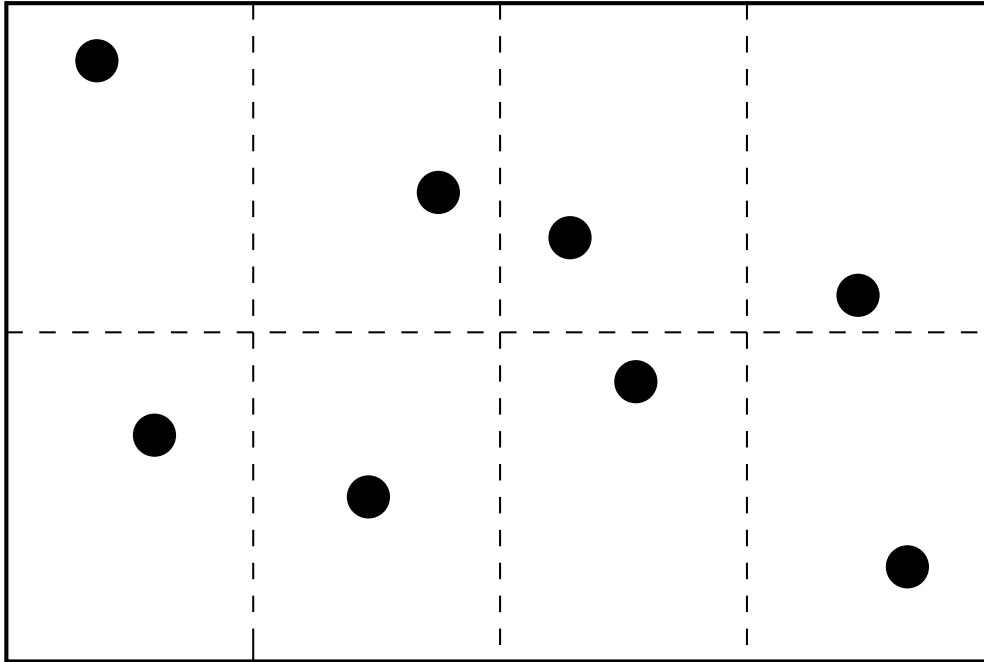
Figure 3: Schematic of a stratified random sampling plan. A structural element is sub-divided (dashed lines) into subsections. Samples (filled circles) are taken from random locations within each subsection.

calculations (a single calculation based on the "best" input parameter values) are limited in their ability to formulate an uncertainty statement. These probabilistic calculations are composed of repeated deterministic calculations where the input parameters are chosen at random from a statistical distribution. The resulting values form a distribution of service lifetimes. The statistical, regulatory, and engineering advantages of probabilistic calculations are significant. The results are rational, defensible statements about the expected performance of a structure.

Unfortunately, relatively little discussion has been made about the commensurate sampling requirements. Probabilistic performance assessment software can conduct an arbitrary number of Monte Carlo calculations based on parameter uncertainty. Increasing the number of Monte Carlo iterations N_{MC} exposes the "tails" of the service life distribution. In cases where the analytical expression for the output distribution is unknown (virtually all the time), the minimum characterizable percentile of the output distribution is proportional to $1/N_{MC}$. Therefore, as one desires information about smaller and smaller percentiles of the service life distribution, one simply increases the number of Monte Carlo calculations.

This approach has an important consequence. As the number of Monte Carlo iterations N_{MC} increases to better characterize the limits of the output distribution, one must be sure that the "tails" of the input parameters are suitably characterized. Although the measured values of the parameters are characterized by a probability distribution,

there is uncertainty in the distribution parameters (confidence interval) due to the finite sample size. Distribution parameters based on a relatively small number of samples could have relatively large uncertainties, resulting in a significant change in the location of the "tail" percentiles.

4.3   Sample Size Effect

Assuming that a suitable distribution for the material property values has been found, the distribution parameters will be estimated from a number of specimens taken from a structure. For the normal distribution, the parameters are the mean and standard deviation. Because these parameters are estimated from a finite sample size, there is an estimable level of uncertainty in these parameters. These uncertainties should then be reflected in the final Monte Carlo calculation.

In principle, the uncertainty in the parameters can be introduced into the Monte Carlo method in a straightforward way. As an example, consider the normal distribution, the parameters of which are the mean and standard deviation. To perform the Monte Carlo calculation, one begins with a normal $N(0, 1)$ random deviate Z and calculates a material property random deviate Y:

$$Y = \mu + \sigma Z \tag{17}$$

where μ and σ are the true mean and standard deviation, respectively. Unfortunately, because the total population is greater than the sample population, the true mean and standard deviation are unknowable, and can only be estimated from the mean $\overline{x}$ and standard deviation s calculated from the n individual measurements x_i:

$$\overline{x} = \frac{1}{n} \sum_{i=1}^{n} x_i \qquad\qquad s = \frac{1}{n-1} \sum_{i=1}^{n} (x_i - \overline{x})^2 \tag{18}$$

To calculate a random material deviate, one uses these estimated parameters:

$$Y = \overline{x} + sZ \tag{19}$$

There is, however, uncertainty in the estimated parameters, and the true mean and standard deviation might differ significantly from the estimated values. Fortunately, the relationship between the estimated and true parameters can themselves be characterized by probability distributions.

4.3.1   Chi-square distribution

When the standard deviation of a sample is estimated from a finite number of observations, the estimated standard deviation s generally differs from the true standard deviation σ. For a sample of n observations from which the standard deviation was calculated, let v represent a ratio of estimated to true values:

$$v = \frac{n\, s^2}{\sigma^2} \tag{20}$$
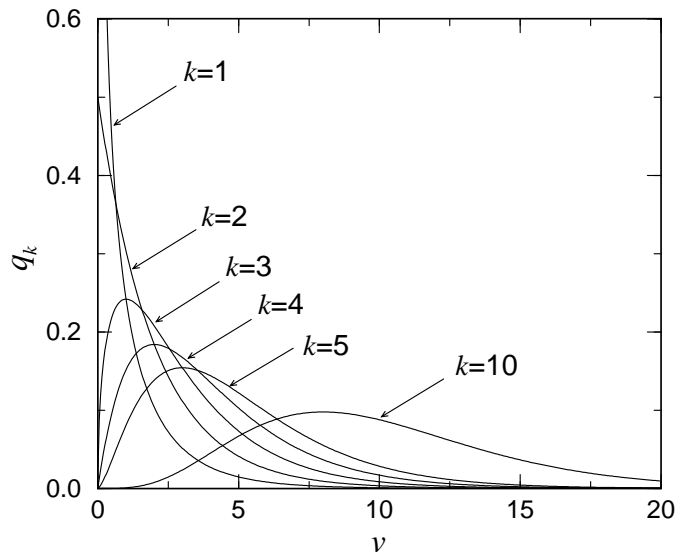
Figure 4: Chi-square distribution $g_k(v)$ for different degrees of freedom k.

Values of this ratio v obey a Chi-square distribution g_k with $(k = n - 1)$ degrees of freedom:

$$g_k(v) = \frac{v^{k/2-1}\, e^{-v/2}}{2^{k/2}\, \Gamma(k/2)} \tag{21}$$

The distribution g_k is shown in Fig. 4 for different values of k. For small values of k, the most probable outcome is to underestimate the true standard deviation. As the number of observations increases, the most probable outcome is to accurately estimate the true standard deviation.

Using a Chi-square random deviate V with k degrees of freedom, a randomized standard deviation σ' that incorporates the uncertainty due to finite sample size can be calculated from the sample standard deviation s:

$$\sigma' = \frac{s}{\sqrt{V/n}} \tag{22}$$

4.3.2 Student t-distribution

When the mean of a population $\overline{x}$ is estimated from a finite number of observations, the estimated mean $\overline{x}$ generally will differ from the true mean μ. For a sample of n observations from which the arithmetic mean is calculated, let t represent the difference between the estimated and true means:

$$t = \frac{\overline{x} - \mu}{s/\sqrt{n}} \tag{23}$$

19
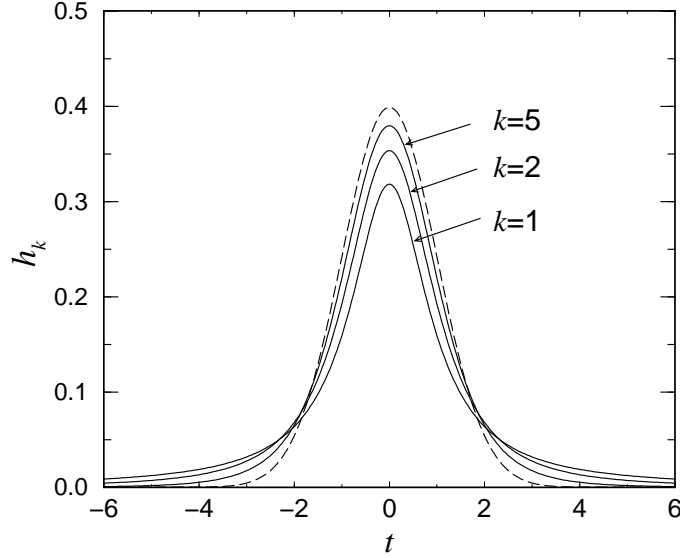
Figure 5: Student t-distribution $h_k(t)$ for 1, 2, and 5 degrees of freedom k. The dashed line is the $N(0,1)$ distribution.

Values of t obey a Student t-distribution h_k with $(k = n - 1)$ degrees of freedom:

$$h_k(t) = \frac{\Gamma\left[(k+1)/2\right]}{\Gamma(k/2)\sqrt{\pi k}} \left(1 + \frac{t^2}{k}\right)^{-(k+1)/2} \tag{24}$$

In the limit $k \to \infty$, the h_k approaches the normal distribution with mean 0 and variance 1: $N(0,1)$.

The Student t-distribution h_k is shown in Fig. 5 for different values of k; the normal $N(0,1)$ is also shown as a dashed line as a reference.

This uncertainty can be built into the estimated mean. Using a Student-t random deviate T with k degrees of freedom, a randomized mean μ' can be calculated from the estimated mean $\overline{x}$ and estimated standard deviation s:

$$\mu' = \overline{x} + T\frac{s}{\sqrt{n}} \tag{25}$$

4.3.3 Adjusted Distribution

The random material deviate Y accounts for finite sample size by combining the Chi-square adjustment to the sample standard deviation s and the Student-t adjustment to the sample mean $\overline{x}$. The final expression starts with the ideal relationship of Eqn. 17 and substitutes the adjusted standard deviation σ' (Eqn. 22) and the adjusted mean μ'

(Eqn. 25):

$$Y = \mu' + Z\sigma' \tag{26}$$

$$= \left(\overline{x} + \frac{sT}{\sqrt{n}}\right) + \frac{Zs}{\sqrt{V/n}}$$

This expression is a function of the measured quantities $\overline{x}$ and s, and the random deviates T (Student-t), Z (normal $N(0,1)$), and V (Chi-square), and the number of observations n.

4.4 Analytical Representation

The effect of finite sample size can be examined analytically for a material parameter characterized by a normal distribution $f(x; \mu, \sigma)$:

$$f(x; \mu, \sigma) = \frac{\exp\left[-\frac{1}{2}\left(\frac{x-\mu}{\sigma}\right)^2\right]}{\sqrt{2\pi}\,\sigma} \tag{27}$$

The distribution that accounts for the finite sample size is calculated by integrating over the possible values of μ and σ. These possible values depend on the sample size and the calculated mean $\overline{x}$ and standard deviation s. Let $\text{pdf}(\mu; \overline{x})$ and $\text{pdf}(\sigma; s)$ represent the PDFs of the mean μ and standard deviation s. The final distribution $p(y; \overline{x}, s)$ is calculated by integrating over the possible values for μ and σ [20]:

$$p(y; \overline{x}, s) = \int_{\mu, \sigma} f(y; \mu, \sigma)\, \text{pdf}(\mu; \overline{x})\, \text{pdf}(\sigma; s)\, d\mu\, d\sigma \tag{28}$$

Ignoring the effects of finite sample size, and assigning $\overline{x}$ and s to μ and σ, respectively, is mathematically equivalent to using the delta function for the respective PDF:

$$\text{pdf}(\mu; \overline{x}) = \delta(\mu - \overline{x}) \qquad\qquad \text{pdf}(\sigma; s) = \delta(\sigma - s) \tag{29}$$

Substituting these distributions into Eqn. 28 yields the normal distribution:

$$p(y; \overline{x}, s) = f(y; \overline{x}, s) \tag{30}$$

This is the typical way of generating random material parameters, but does not account for the finite sample size, and the commensurate uncertainty in the estimated mean and standard deviation.

Accounting for finite sample size requires the appropriate PDF for μ and σ. The appropriate distributions are the Student t and Chi-square, respectively:

$$\text{pdf}(\mu; \overline{x}, s)\, d\mu = h_k(t)\left|\frac{dt}{d\mu}\right| d\mu \qquad\qquad \text{pdf}(\sigma; s)\, d\sigma = g_k(v)\left|\frac{dv}{d\mu}\right| d\mu$$

$$= h_k\left(\frac{x - \mu}{s/\sqrt{n}}\right)\left|\frac{-\sqrt{n}}{s}\right| d\mu \qquad\qquad = g_k\left(n\frac{s^2}{\sigma^2}\right)\left|\frac{2ns^2}{\sigma^3}\right| d\sigma$$

Substituting into Eqn. 28 yields the complete expression for the integral:

$$p(y; \overline{x}, s) = \int_{\mu, \sigma} f(y; \mu, \sigma) \, h_k \left(\frac{\overline{x} - \mu}{s/\sqrt{n}} \right) \, g_k \left(n \frac{s^2}{\sigma^2} \right) \, \left(\frac{2n^{3/2}s}{\sigma^3} \right) \, d\mu \, d\sigma \qquad (31)$$
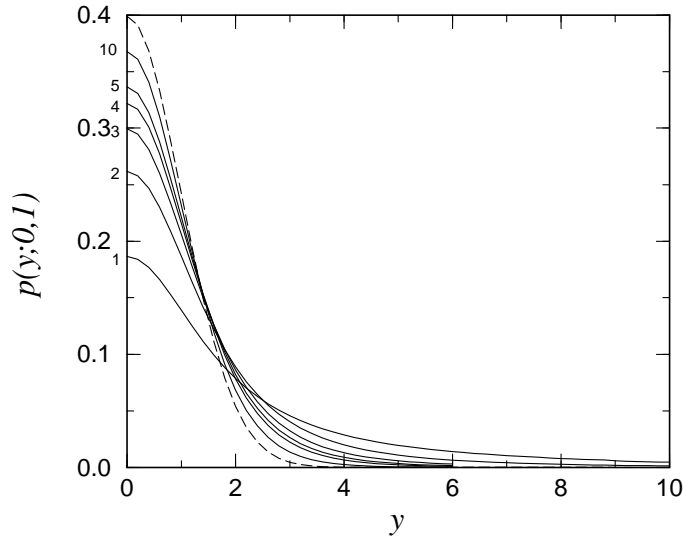
Figure 6: Modified material parameter distribution to account for finite sample size. The degrees of freedom k are labeled along the ordinate. The dashed line denotes the N(0,1) distribution.

As a demonstration, the distribution $p(y; \overline{x} = 0, s = 1)$ is plotted in Fig. 6 for different degrees of freedom. Because the function $p(y; \overline{x}, s)$ is symmetric about $y = 0$, it is plotted only for positive values of y to show detail. Also in Fig. 6 is the normal $N(0, 1)$ distribution, shown as the dashed line. As the number of observations increases, the output function approaches that of the normal distribution. For small numbers of observations, however, the distribution is considerably wider than the normal distribution.

4.5   95-th Quantile

The effect of sample size on the probability of obtaining large values can be substantial. Consider, as an example, the 95-th quantile $y_{.95}$ of $p(y; \overline{x}, s)$:

$$0.95 = \int_{-\infty}^{y_{.95}} p(y; \overline{x}, s) \, dy \qquad (32)$$

Therefore, 5 % of the random values will be larger than $y_{.95}$.

The values of $y_{.95}$ for varying degrees of freedom k are shown in Table 1, and are plotted as a function of k^{-1} in Fig. 7. Also shown in the table are the corresponding Student-t statistic $t_{.95}$ and the ratio of the Chi-square statistic to the degrees of freedom

22
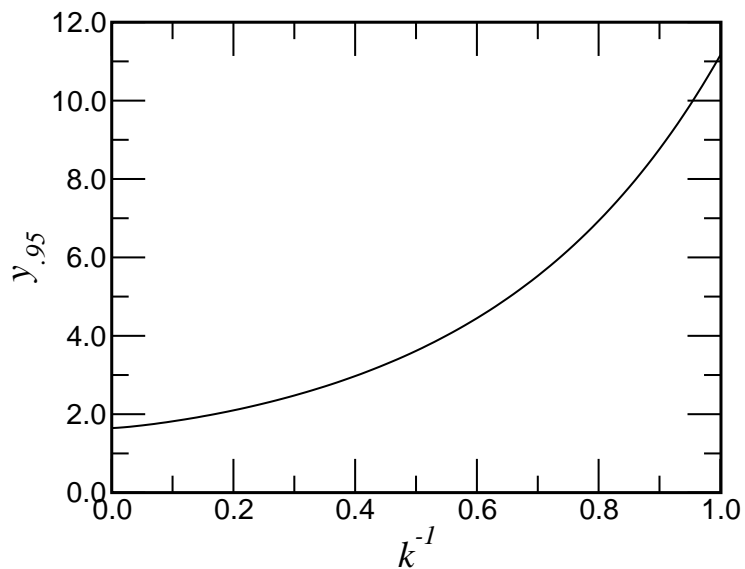
Figure 7: $y_{.95}$ as a function of the degrees of freedom k.

$\chi^2_{.95}/k$. The value of $y_{.95}$ is greater than either of the other statistics. Therefore, using either statistic by itself would not fully capture the effect of sample size.

In effect, the ratio $y_{.95}/1.65$ is the multiplier by which the 95-th quantile changes with respect to k. For $k = \infty$, the value of $y_{.95}$ is equal to the 95-th quantile of the normal distribution. At $k = 1$, the value of $y_{.95}$ has increased by a factor of seven.

Table 1: The 95-th quantile $y_{.95}$ for the distribution $p(y; \overline{x}, s)$. Also shown are the Student-t statistic $t_{0.95}$ and the ratio of the Chi-square statistic to the degrees of freedom $\chi^2_{.95}/k$.

k	$y_{.95}$	$t_{.95}$	$\chi^2_{.95}/k$
1	11.29	6.31	3.84
2	3.67	2.92	3.00
3	2.73	2.35	2.60
4	2.40	2.13	2.37
5	2.20	2.02	2.21
10	1.90	1.81	1.83
20	1.77	1.73	1.57
∞	1.65	1.65	1.00

5 Example

To demonstrate the assessment method, a fictitious scenario will be developed and analyzed in this Section. The service life of the element will be based on the initiation of corrosion in the internal steel elements. The corrosion model is considered because the sulfate model is empirical, giving only the rate of sulfate erosion, and failure due to leaching is an extremely long term failure mechanism.
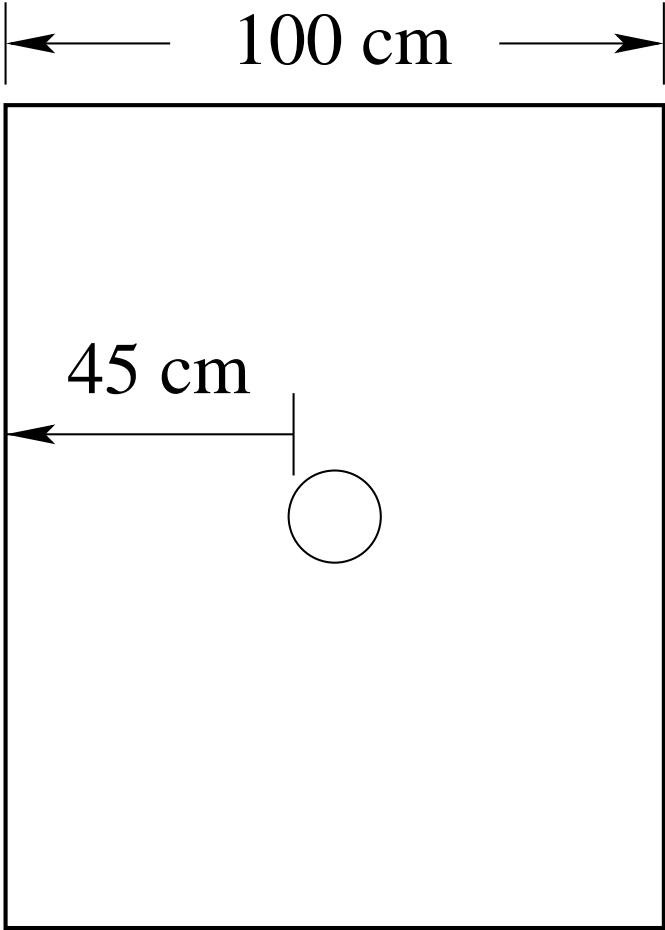
Figure 8: Example scenario showing 100 cm thick wall with 10 cm diameter reinforcement gallery in the center.

5.1 Scenario

The example concrete element will be a wall that is 1 m thick. In the middle of the element is a steel post-tensioning gallery. A schematic of the system is shown in Fig. 8. The element will be exposed to ground water containing sodium chloride. The service life will be the time required for a sufficient concentration of chlorides to initiate corrosion

in the steel gallery. For the 4SIGHT model, the critical chloride concentration is that at which the ratio of chlorides to hydroxyls ($[Cl^-]/[OH^-]$) is greater than 0.6.

5.2 Concrete Mixture

Table 2: Input parameters to the ACI 211 mixture design procedure.

Property	Value
Compressive Strength	30 MPa
Maximum Aggregate Size	25 mm
Coarse Aggregate Density	2800 kg/m^3
Fine Aggregate Density	2600 kg/m^3
Element Type	Mass Concrete
Air Entrainment	Moderate Exposure

The concrete mixture used in this example was obtained from an ACI 211 mixture design calculation. The concrete is composed of ordinary portland cement (OPC), with no supplemental pozzolanic mineral admixtures. The structure is to be exposed to freezing and thawing, so air entrainment is required. The input parameters to the ACI 211 calculation are given in Table 2.

The output from the ACI 211 mixture design calculation is shown in Table 3. The ACI 211 design code is only meant as a useful starting point in designing a mixture. Therefore, the fact that the volume fractions do not sum to one is not a great concern. They are still useful as a starting point for this example calculation. In practice, the analyst has the actual mixture design from which to calculate the appropriate volume fractions. These estimates can be verified independently from a petrographic examination of a polished concrete section.

Table 3: Concrete mixture design based on ACI 211 for normal strength concrete. The corresponding w/c is 0.45, and the estimated slump is 51 mm.

Material	kg/m^3	Volume Fraction
Water	164	0.164
Cement	365	0.114
Coarse Agg.	966	0.345
Fine Agg.	899	0.345
Entrained Air		0.045

5.3 Material Parameters

A number of material parameters are required to perform a 4SIGHT calculation. In most cases, these parameters can be estimated from the mixture design. Direct measurement, however, is the preferred method.

5.3.1 Capillary Porosity

The capillary porosity ϕ can be estimated using the water:cement ratio ϵ and the degree of hydration α [1]:

$$
\begin{aligned}
\phi &= 1 - \frac{1 + 1.16\alpha}{1 + 3.2\epsilon} \\
&= 0.162
\end{aligned}
\tag{33}
$$

For this calculation, it is assumed that the degree of hydration α is 0.90, which should be reasonable for a 30 year old concrete structure. This value for the capillary porosity is used as input to the 4SIGHT calculation, and will be useful in subsequent calculations.

5.3.2 Formation Factor

There are at least two ways to estimate the concrete formation factor. The first is to use the model of Bentz et al. [21, 22] that requires the water:cement ratio ϵ, the degree of hydration α, and the volume fraction of aggregate (0.690). The calculation can be performed using the Virtual Cement and Concrete Testing Laboratory (VCCTL) web site (`http://vcctl.cbt.nist.gov`).

Strictly speaking, the VCCTL web site returns an estimate for the chloride diffusion coefficient. This value will be converted to an estimate for the formation factor by using the self-diffusion coefficient of chloride at 25 °C [23] (2.03×10^{-9} m^2/s). For this mixture design, the estimated chloride diffusion coefficient is 9.3×10^{-13} m^2/s. The corresponding formation factor is the ratio of the chloride self-diffusion coefficient to this value:

$$
F = \frac{2.03 \times 10^{-9}}{9.3 \times 10^{-13}} = 2183
\tag{34}
$$

This value can be checked for consistency using a model for the formation factor of a paste and Archie's law. A model for estimating the formation factor of a paste F_{paste} was developed [13, 24] that is a function of only the capillary porosity ϕ:

$$
\begin{aligned}
F_{paste}^{-1} &= 0.001 + 0.07\phi^2 + 1.8(\phi - 0.18)^2 \mathrm{H}(\phi - 0.18) \\
&= 0.00284 \\
&= (352)^{-1}
\end{aligned}
\tag{35}
$$

The function $\mathrm{H}(x)$ is the Heaviside function (and equals zero in this case because the estimated porosity from Eqn. 33 is less than 0.18). The paste formation factor F_{paste} is approximately 352. The volume fraction of paste v_{paste} within the concrete is 0.265.

Based on Archie's law, the formation factor for the concrete F_{conc} is a function of the paste formation factor and the volume fraction of paste:

$$F_{conc} \approx F_{paste} v_{paste}^{-1.5} = 2580 \tag{36}$$

This value is consistent with the formation factor of 2183 reported by the VCCTL model.

In addition to an estimated diffusion coefficient, the VCCTL model also gives an interval ($[4.7,18.0] \times 10^{-13}$ m^s/s) having a 90 % coverage factor. The corresponding 90 % coverage for formation factor $F_{.90}$ can be calculated in a manner similar to Eqn. 34 above:

$$F_{.90} = \frac{2.03 \times 10^{-9}}{[4.7, 18.0] \times 10^{-13}} = [1128, 4319] \tag{37}$$

This information is sufficient to now examine a suitable distribution function to characterize the formation factor uncertainty.

A suitable distribution can be found by considering the midpoint of the $F_{.90}$ range. The midpoint of the range is 2723, which differs significantly from the estimated value 2183. Consider, however, the logarithm (base 10) of the values:

$$\log F = 3.34 \qquad\qquad \frac{\log 4319 + \log 1128}{2} = 3.34$$

Therefore, the logarithms of the range $F_{.95}$ are symmetric about the logarithm of the predicted value. We conclude that the formation factor uncertainty is best characterized by a lognormal distribution. The remaining task is to determine some characteristic standard deviation.

The standard deviation can be approximated from a comparison between the 90 % coverage and two standard deviations. Two standard deviations, for a normal distribution, has a coverage of approximately 95 %. The scaling between the 90 % coverage range $F_{.90}$ and two standard deviations can be approximated by the ratio of the corresponding quantiles of the normal distribution:

$$\log F_{.95} \approx \log F_{.90} \frac{1.960}{1.645} \tag{38}$$

Moreover, an estimate of one standard deviation would be one quarter of this new range:

$$\sigma = \frac{[\log 4319 + \log 1128] \left(\frac{1.960}{1.645}\right)}{4} = 0.174 \tag{39}$$

The final result is that the formation factor can be characterized by the following relationship:

$$F = 10^{3.34 \pm 0.174} \tag{40}$$

The uncertainty represents one standard deviation, as required for the **4SIGHT** input.

5.3.3 Permeability

An approximation for the permeability can be estimated from an analytical relationship [1] that was developed from the review article by Hearn [10]:

$$k \approx 10^{5.0\epsilon - 21} \text{ m}^2 \tag{41}$$

Based on the data shown in Figure 20 of Hearn, a coverage of 95 % would span approximately three orders of magnitude. Given this, and given that the uncertainty in the permeability is best approximated by the lognormal distribution, the permeability can be easily expressed:

$$k = 10^{-18.75 \pm 0.75} \text{ m}^2 \tag{42}$$

The uncertainty represents one standard deviation.

5.4 Pore Solution

The composition of the pore solution can be approximated using the work of both Taylor [14] and Reardon [25]. To simplify the analysis, it is assumed that only the potassium, sodium, sulfate, and hydroxide concentration are significant. Although the oxide contents of a cement are easily determined, for the sake of this example, the following oxide mass fractions are used (see column one of Table 3 in Ref. [25]):

Oxide	Mass Fraction
K_2O	1.18
Na_2O	0.41

These oxide contents can then be combined with Taylor's model [14] for predicting the pore solution composition. The analysis is based on a 100 g sample of cement. The corresponding number of moles of sodium and potassium in the sample are as follows:

Element	moles per 100 g cement
K	0.0251
Na	0.0132

According to the Taylor model, the analyst determines the fraction of each cement mineral species that has reacted. Because it is assumed that the degree of hydration is 0.90, the calculation is simplified by assuming the quantity of each elemental species released into the pore solution is equal to the total number of moles present.

The concentrations of the potassium and sodium ionic species is the ratio of the moles of element released m_r to a corrected volume of water. The correction first accounts for the volume of bound water V_b and then adjusts for binding of species b into the hydration products:

$$c(\text{mol}/100 \text{ g H}_2\text{O}) = \frac{m_r}{100\epsilon - V_b + b}$$

The volume of bound water V_b from a fully hydrated 100 g cement sample is approximately 31.6 cm^3 [14]. The species binding parameters are the following [14]:

Species	b (cm^3)
K$^+$	20
Na$^+$	31

Upon substitution for these quantities, the final estimates for the concentrations are as follows:

Species	Molality (mol/kg$_w$)
K$^+$	0.654
Na$^+$	0.267

According to Taylor, the sulfate concentration can be approximated from the potassium and sodium concentrations:

$$m_{SO_4^{2-}} \approx 0.06 \left(m_{K^+} + m_{Na^+} \right)^2 = 0.051 \text{mol/kg}_w$$

5.5 Portlandite Content

It is assumed that every 100 g of cement (in the absence of supplemental pozzolanic mineral admixtures) will produce 30 g of portlandite. Based on this assumption, the concentration of portlandite produced, per kg water, can be approximated from the water:cement ratio ϵ:

$$m_{Ca(OH)_2} \approx \frac{4.05}{\epsilon} \text{ mol/kg}_w$$

For the 0.45 water:cement ratio used here, the expected portlandite concentration is 9.0 mol/kg$_w$.

5.6 Cracks

For the purpose of this example, it will be assumed that cracks are detected in the concrete element. The cracks are approximately 100 μm wide, spaced 10 m apart, and extend into the wall to a depth that is approximately 40 % of the entire wall thickness. The standard deviation of crack thickness is 25 μm, and the uncertainty in the crack penetration depth is ± 20 % of the wall thickness; the standard deviation is assumed to be one half this, or 0.10. Using the aforementioned information, the ratio of the bulk permeability (intact concrete plus cracks) to the intact concrete is a factor of 1.67.

5.7 Negative Internal Hydrostatic Pressure

For this example, it will be assumed that the interior of the structure will be maintained at a negative pressure approximately equal to 10132 Pa (0.1 atm). Analysis will be performed with both no pressure difference, and the 10.1 kPa difference for comparison purposes.

5.8 Exposure

The exposure condition is assumed to be a brackish groundwater. As a reference, exposure to seawater is also considered. In every case, the exposure concentration is assumed to be constant over the life of the concrete element.

Table 4: Seawater composition based on Schlesinger (Table 9.1, p. 263). The brackish water has a salinity of approximately 3.5 g/kg.

	Seawater		Brackish
Species	mg/kg	mol/L	mol/L
Cl^-	19350	0.546	0.0546
Na^+	10760	0.468	0.0468
SO_4^{2-}	2712	0.028	0.0028
Mg^{2+}	1294	0.053	0.0053
Ca^{2+}	412	0.010	0.0010
K^+	399	0.010	0.0010

The composition of seawater is fairly constant throughout the world, with the salinity varying from 30 g/kg to 40 g/kg [26]. On the Atlantic and Pacific coasts of the United States, the salinity is approximately 35 g/kg and 34 g/kg, respectively (See Reference [26], Figure 9.3, p. 259).

The particular seawater composition used here is shown in Table 4. Although additional diffusing species are given in the reference, only species appearing at a concentration of at least 0.010 mol/L are included.
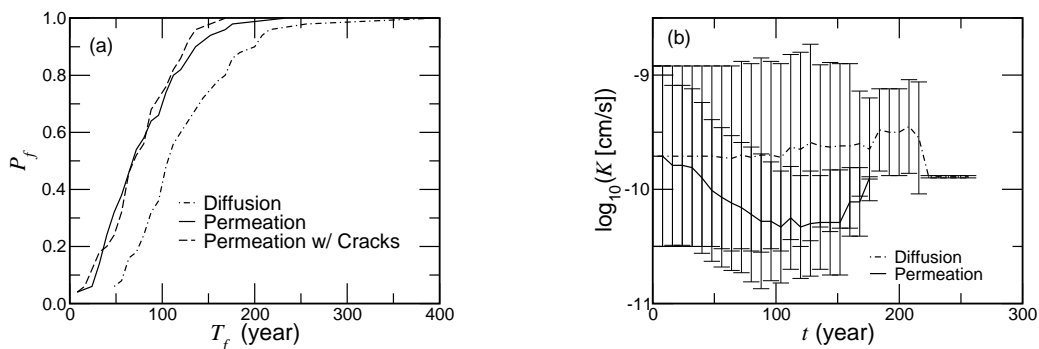

Figure 9: Response of concrete exposed to seawater: (a) Probability of failure P_f as a function of the failure time T_f; and (b) The logarithm of hydraulic conductivity K as a function of of time t. The error bars represent one standard deviation.

5.9 Results

For both the seawater and brackish water exposures, different combinations of diffusive and advective transport are studied; advective transport is achieved by applying a 10.1 kPa negative pressure within the structure's interior. For the advective transport, both cracked and uncracked concretes are considered.

For each combination of exposure and transport, the calculation is repeated 50 times to obtain useful statistics. For each iteration, the time to failure T_f (the initiation of corrosion) is recorded. These values are sorted in ascending order and plotted against their ordinal value. The result is a cumulative probability plot, as a function of time t, for the fraction of systems that failed before time t.

In addition, for each of the 50 iterations, the bulk permeability is calculated periodically. The mean and standard deviation of the bulk permeability at time t are calculated from the population of 50. This gives, in effect, the time-dependent behavior for the bulk permeability.

5.9.1 Seawater Results

Exposure to seawater is used as a reference. The probability of failure P_f and the logarithm of the hydraulic conductivity K as a function of time are shown in Fig. 9 as a function of time. The results for the case of no negative internal pressure are shown as the "Diffusion" curve in Fig. 9(a). In the presence of a pressure head, but in the absence of cracks, the probability of failure, at a give time, increases dramatically, as expected. Because the effect of the cracks is to increase the permeability by a factor 1.67, the effect of cracks is small by comparison to the other variables.

The evolution of the bulk hydraulic conductivity K over time, as shown in Fig. 9(b) is revealing. For each of the 50 iterations, the logarithm of the bulk hydraulic conductivity was recorded as a function of time. The average logarithm is shown, along with the standard deviation of the logarithms. Although the error bars overlap, the deviations are symmetric about the average value.

The interesting feature to note is that, although the duration of the service life decreased with the addition of permeation, the bulk hydraulic conductivity also decreased. This occurs because, as the portlandite is leached from the concrete, the Darcy flow carries the excess calcium ions deeper into the concrete, where they reprecipitate, decreasing the porosity. The region within the concrete having the decreased porosity also has a decreased permeability. In cases with 1-D flow, if any portion of the system has a low permeability, it will have a dramatic effect on the overall bulk permeability.

5.9.2 Brackish Results

The results for the calculations using the brackish water exposure are shown in Fig. 10. Because a brackish exposure is more likely than a seawater exposure, a number of additional scenarios were considered.

In Fig. 10(a), the failure probability increases as the systems advance from purely diffusive D systems, to permeative K systems. The dot-dash system is purely diffusive,
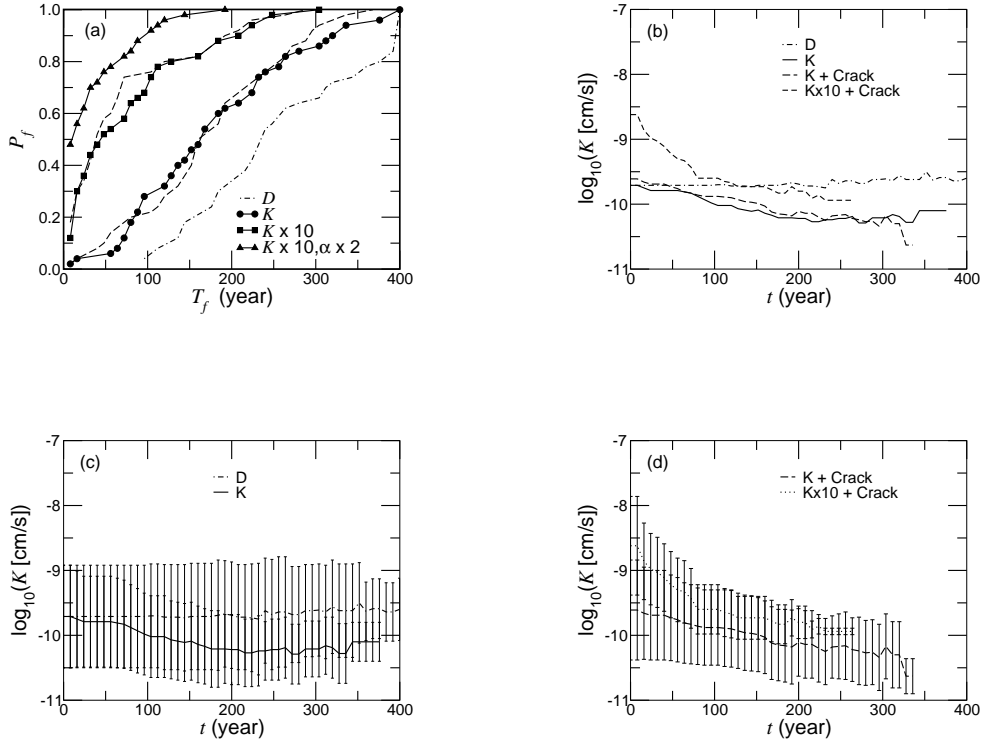
Figure 10: Response of concrete exposed to brackish water (salinity: 3.5 g/kg): (a) Probability of failure P_f as a function of failure time T_f. Permeating systems shown with solid lines and the addition of cracks denoted by the dashed line in proximity to the solid line system; and (b) The logarithm of hydraulic conductivity K as a function of of time t (mean values shown); and (c,d) The logarithm of the hydraulic conductivity K, as in (b). Error bars represent one standard deviation.

and has the lowest probability of failure. With the addition of a pressure head (solid curve with filled circles), the failure probability increases. Interestingly, adding cracks (dashed line) again does not change the results appreciably for the reason mentioned previously.

Increasing the concrete permeability (in the absence of cracks) by a factor of ten increased the failure probability considerably. As in the previous case, however, the addition of cracks (dashed line) did not change the failure probability appreciably.

While the transition from a permeating system to a permeating system with cracks penetrating 40 % of the concrete thickness did not change the response appreciably, the extension of the cracks to 80 % of the concrete thickness (dot-dash line) did have a noticeable effect on the failure probability.

The time dependence of the bulk hydraulic conductivity K, shown in Figs. 10(b-d),

exhibits behavior similar to the seawater scenario. The diffusive systems exhibited virtually no change in the bulk hydraulic conductivity. The addition of a Darcy flow, however, decreased the bulk hydraulic conductivity for the same reasons as for the seawater case.

It should be noted that changes in the bulk permeability can be achieved only through changes in the total capillary porosity due to salt dissolution and precipitation. Presently, corresponding changes in the transport coefficients are based solely on changes in the capillary porosity of the intact concrete and not changes in the transport properties of the cracks. Additional work is needed to consider transport in the intact concrete and the cracks separately so that the effects of dissolution/precipitation on the crack transport properties can be incorporated into changes in the transport coefficients.

6 Summary

A performance assessment method has been described and demonstrated for cement-based structures considered for entombment. The assessment relies upon careful characterization of both the material properties of the intact concrete and the following crack properties: crack width, crack spacing, and crack penetration depth. In addition, the uncertainty in each material property is incorporated into a Monte Carlo calculation incorporating parameter uncertainty.

The effects of cracks can be extensive. A sensitivity analysis shows that crack width and relative crack penetration depth have the greatest effect on bulk permeability. Given the same relative change in the two crack properties, the crack penetration depth has the greatest effect on the bulk properties. Therefore, the development of nondestructive techniques for characterizing crack properties should concentrate on accurate determination of the crack penetration depth.

To address uncertainty in the material parameters, guidelines for sampling and for distribution characterization have been discussed. The proposed sampling strategy considers both the spatial distribution of the sampling and the uncertainty due to a finite number of samples; the mean comes from the Student t-distribution and the standard deviation comes from the Chi-Square distribution, both with a number of degrees of freedom that depends upon the sample size. Analysis shows that very small sample size can dramatically increase the uncertainty in the calculated distribution parameters. A measure of this effect was demonstrated by calculating the 95-th percentile of the sample distribution as a function of the number of degrees of freedom. For the case of only two samples, the distance between the mean and the 95-th percentile increases by a factor of seven.

An example assessment was calculated for exposure to a brackish groundwater with a salinity of 3.5 g/kg (seawater is typically 35 g/kg). The estimated time until the onset of corrosion was calculated for different transport modes: diffusion; diffusion and permeation through intact concrete; diffusion and permeation through cracked concrete. For each scenario considered, the calculation was repeated 50 times, each time incorporating material parameter uncertainty, to yield a statistical statement about the expected lifetime before corrosion initiation. While the addition of cracks to the calculation always increases the bulk permeability, the changes in the service life were not distinguishable for cracks penetrating to 40 % of the element thickness.

The long-term behavior of the bulk permeability of diffusion systems remained virtually constant throughout their service life. The permeability of systems undergoing Darcy flow decreased over time. The decrease was due to the dissolution of calcium hydroxide at the surface and transport of calcium ions into the concrete. Deeper in the concrete, the higher pH re-precipitated the calcium hydroxide, reducing the porosity, and thereby reducing the bulk permeability. Because of this type of effect, the behavior of cracks during dissolution/precipitation may be very important, and warrants further research.

References

[1] K. A. Snyder and J. R. Clifton. `4SIGHT` manual: A computer program for modeling degradatation of underground low level waste concrete vaults. Technical Report NISTIR 5612, National Institute of Standards and Technology, Gaithersburg, MD, 1995.

[2] K. A. Snyder. Validation and modification of the `4sight` computer program. Technical Report NISTIR 6747, National Institute of Standards and Technology, Gaithersburg, MD, 2001.

[3] K. A. Snyder and J. Marchand. Effect of speciation on the apparent diffusion coefficient in nonreactive porous systems. *Cem. Concr. Res.*, 31:1837–1845, 2001.

[4] M. J. Lighthill. *Introduction To Fourier Analysis and Generalised Functions*. Cambridge University Press, Cambridge, ENGLAND, 1958.

[5] W. F. Espenscheid, M. Kerker, and E. Matijević. Logarithmic distribution functions for colloidal particles. *J. Phys. Chem.*, 68:3093–3097, 1964.

[6] V. M. Malhotra and N. J. Carino, editors. *CRC Handbook on Nondestructive Testing of Concrete*. CRC Press, Boca Raton, 1991.

[7] ACI Manual of Concrete Practice. Technical report, American Concrete Institute, Farmington Hills, MI, 2000.

[8] Thierry Bourbie and Joel Walls. Pulse decay permeability: Analytical solution and experimental test. *Society of Petroleum Engineers Journal*, pages 719–721, October 1982.

[9] D. Trimmer. Laboratory measurements of ultralow permeability of geologic materials. *Rev. Sci. Instrum.*, 53:1246–1254, 1982.

[10] N. Hearn, R. D. Hooton, and R. H. Mills. Pore structure and permeability. In P. Klieger and J. F. Lamond, editors, *Significance of Tests and Properties of Concrete and Concrete-Making Materials*, ASTM STP 169C, pages 240–262. American Society for Testing and Materials, Philadelphia, PA, 1994.

[11] R. S. Barneyback Jr. and S. Diamond. Expression and analysis of pore fluid from hardened cement pastes and mortars. *Cement and Concrete Research*, 11:279–285, 1981.

[12] K. A. Snyder, C. Ferraris, N. S. Martys, and E. J. Garboczi. Using impedance spectroscopy to assess the viability of the rapid chloride test for determining concrete conductivity. *Journal of Research of the National Institute of Standards and Technology*, 105:497–509, 2000.

[13] D. P. Bentz. CEMHYD3D: A three-dimensional cement hydration and microstructural development modelling package. version 2.0. Technical Report NISTIR 6485, National Institute of Standards and Technology, Gaithersburg, MD, April 2000.

[14] H. F. W. Taylor. A method for predicting alkali ion concentrations in cement pore solutions. *Advances in Cement Research*, 1:5–16, 1987.

[15] K. A. Snyder. Effect of drying shrinkage cracks and flexural cracks on concrete bulk permeability. Technical Report NISTIR 6519, National Institute of Standards and Technology, Gaithersburg, MD, 2000.

[16] Guide to the expression of uncertainty in measurement. Technical report, International Organization for Standardization (ISO), Genève, Switzerland, 1993.

[17] B. N. Taylor and C. E. Kuyatt. Guidelines for evaluating and expressing the uncertainty of nist measurement results. Technical report, National Institute of Standards and Technology, Gaithersburg, Maryland, 1993.

[18] E. B. Wilson. *An Introduction to Scientific Research*. McGraw-Hill, 1952.

[19] J. R. Taylor. *An Introduction to Error Analysis*. University Science Books, second edition, 1997.

[20] P. L. Meyer. *Introductory Probability and Statistical Applications*. Addison-Wesley, Reading, second edition, 1970.

[21] D. P. Bentz, R. J. Detwiler, E. J. Garboczi, P. Halamickova, and L. M. Schwartz. Multi-scale microstructural modeling of the diffusivity of mortar and concrete. In *RILEM International Conference on Chloride Penetration into Concrete*. RILEM, 1995.

[22] D. P. Bentz, E. J. Garboczi, and E. S. Lagergren. Multi-scale microstructural modeling of concrete diffusivity: Identification of significant variables. *Cement and Concrete Research*, 20:129–139, 1998.

[23] R. Mills and V. M. M. Lobo. *Self-Diffusion in Electrolyte Solutions*. Elsevier, New York, 1989.

[24] D. P. Bentz and G. P. Forney. User's guide to the nist virtual cement and concrete testing laboratory. version 1.0. Technical Report NISTIR 6583, National Institute of Standards and Technology, Gaithersburg, MD, November 2000.

[25] E. J. Reardon. Problems and approaches to the prediction of the chemical composition in cement/water systems. *Waste Management*, 12:221–239, 1992.

[26] W. H. Schlesinger. *Biogeochemisry: An Analysis of Global Change*. Academic Press, San Diego, 1991.